Polymer 50 (2009) 4250–4256

Contents lists available at ScienceDirect

Polymer

journal homepage: www.elsevier.com/locate/polymer

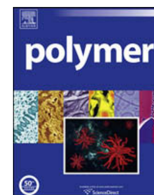

Nine-fold density multiplication of hcp lattice pattern by directed self-assembly of block copolymer

Yasuhiko Tada [a], Satoshi Akasaka [b], Mikihito Takenaka [b,*], Hiroshi Yoshida [a], Ricardo Ruiz [c], Elizabeth Dobisz [c], Hirokazu Hasegawa [b]

[a] *Materials Research Laboratory, Hitachi Ltd., 7-1-1 Omika, Hitachi, Ibaraki 319-1292, Japan*
[b] *Department of Polymer Chemistry, Graduate School of Engineering, Kyoto University, Kyoto-daigaku Katsura, Nishikyo-ku, Kyoto 615-8510, Japan*
[c] *San Jose Research Center, Hitachi Global Storage Technologies, 3403 Yerba Buena Rd., San Jose, CA 95135, USA*

A R T I C L E   I N F O

Article history:
Received 21 May 2009
Accepted 18 June 2009
Available online 24 June 2009

Keywords:
Block copolymer
Thin film
Directed self-assembly

A B S T R A C T

Block copolymer assembly directed by electron beam (EB) lithography enhances both resolution and throughput of the EB-generated patterns and provides a feasible path to fabricating master molds of nanometer scale patterns over macroscopic areas. In our previous paper [27], we demonstrated that the self-assembly process can interpolate points in between the EB-generated pattern, thus attaining four-fold density multiplication. Here, we report a nine-fold feature density multiplication can be attained by the directed block copolymer assembly. The equilibrium formation of perpendicular cylindrical domains in registration with the pre-patterned surface is confined within a narrow thickness range once all other parameters are fixed as found in a four-fold feature density multiplication. The tolerance of the lattice mismatch between chemical pattern and *d* spacing of domains for nine-fold feature density multiplication is smaller than that for four-fold feature density multiplication. We also found that the critical dimension formed by the block copolymer domains is independent of that defined by the EB pre-patterned features.
© 2009 Elsevier Ltd. All rights reserved.

1. Introduction

Demand forever smaller critical dimensions in the semiconductor and storage industries continue pressing conventional photolithography beyond the diffraction limit. Scientific and technological challenges arise as resolution requirements approach molecular length scales and the economics of new lithographic technologies become prohibitively expensive [1,2]. While electron beam (EB) lithography can routinely produce features in the 15–25 nm range (and even down to 2–5 nm [3–5] under special conditions), the application is often limited by low feature densities and low throughput. In this context, self-assembling structures at the nanometer scale have emerged as a way to overcome current lithographic resolution limitations [6–10]. In particular, block copolymer directed assembly with a high density multiplication factor stands out as a promising alternative to overcome EB lithographic resolution and throughput limitations.

Block copolymers exhibit a wide variety of periodic nanodomain structures, such as parallel-oriented lamellar, hexagonally-packed cylinder, and a body centered lattice of spheres [11–15]. Block copolymer thin films deposited onto substrate surfaces, can be utilized as resist patterns that can be transferred into a variety of substrates. Methods, such as graphoepitaxy [16–21] and chemical registration [22–27] have been proposed to precisely control the domain morphology and its orientation to obtain patterns with precision required for lithographic applications. The effect of a chemically-patterned surface template on the orientation of microphase separated diblock copolymer was first reported by Rockford et al. [22]. Nealey et al. have shown directed lamellar- [23] and cylinder- [24,25] microdomains of poly(styrene-*block*-methyl methacrylate) (PS-*b*-PMMA) in registration with the lithographically defined patterns in chemically modified surfaces with a one-to-one correspondence. Recently, Ruiz et al. [26] and Tada et al. [27] successfully demonstrated that areal density of chemical templates can be multiplied by a factor of 4 in hexagonal array patterns. The vertical cylinders filled lattice points halfway between the lattice points on the template pattern. Cheng et al. showed a similar template pattern interpolation for line arrays applying lamellar-forming PS-*b*-PMMA [28]. The combination of chemical registration and self-assembly of block copolymer would enable us to attain higher density multiplication.

In this paper we demonstrate a nine-fold feature density multiplication by directed block copolymer assembly. We clarify the tolerance ranges for nine nine-fold feature density multiplication in

* Corresponding author. Tel.: +81 75 383 2622; fax: +81 75 383 2623.
E-mail address: takenaka@alloy.polym.kyoto-u.ac.jp (M. Takenaka).

0032-3861/$ – see front matter © 2009 Elsevier Ltd. All rights reserved.
doi:10.1016/j.polymer.2009.06.039

terms of film thickness and lattice mismatch and compare the tolerance ranges with those for the four-fold feature density multiplication. We also show that the critical dimension formed by the block copolymer domains is independent of that defined by the EB pre-patterned features.

2. Experimental

Fig. 1 illustrates the density multiplication process. We first prepared hexagonal array of dots on Si substrates by chemical patterning and then the density multiplication was attained by directed self-assemble of block copolymer in thin film.

2.1. Materials

Polystyrene-*block*-poly(methyl methacrylate) (PS-*b*-PMMA) and hydroxy-terminated polystyrene (PS–OH) were purchased from Polymer Source Inc., Quebec, Canada. The weight averaged molecular weight and weight fraction of its PS block were 4.8×10^4 and 0.75, respectively. The weight averaged molecular weight of PS–OH was 3.7×10^3.

2.2. Substrate preparation

Si substrate surfaces were chemically-patterned in the following manner. First the Si substrate was cleaned in a piranha solution at 80 °C for 15 min and rinsed in deionized water. Next, a 1.0 wt% PS–OH solution in toluene was spin-coated onto the Si substrate to a thickness of about 50 nm. The grafting of PS on the Si substrate was completed by annealing the PS–OH-coated Si wafer in vacuum at 140 °C for 48 h. Unreacted PS–OH was removed by rinsing the substrate with toluene. The thickness of PS grafted layer was determined by X-ray reflectometry to be 5.1 nm. Next, the PS-grafted layer was patterned by EB lithography. PMMA resist was spin-coated onto the PS-grafted Si substrate to thicknesses of 50 nm. The samples were exposed by electron beam in hexagonal arrays of dots and developed. Since the dots were exposed by EB, development removed only the dots in the PMMA. Lattice spacings of hexagonal arrays of dots used in this study were slightly around $d_s = 3d_o$, where d_s is the spacing between lattice planes defined by EB on the substrate and d_o is the corresponding natural spacing of the block copolymer in the bulk (See Fig. 1). The samples were subsequently etched by O_2 reactive etching technique (RIE) using a SAMCO RIE-10NR etcher operated at the plasma power of 100 W. The etching time was short, 5 s, so that the PMMA mask remained and only the grafted PS in the holes was selectively reacted with the plasma. The PMMA mask was removed by rinsing the substrate with *N*-methyl-2-Pyrolidone and/or toluene, leaving a chemically-patterned substrate. The treated areas on the substrate have a higher affinity for PMMA while the PS-grafted surface has a weak preferential affinity for PS.

2.3. Sample preparation

Thin films of PS-*b*-PMMA were spin-coated from a dilute solution in toluene. The thickness of the films was controlled by the concentration of the solutions and the spin speed. Spin-coated samples were then annealed at 170 °C for 12 h in vacuum to reach their equilibrium state. Thicknesses of the PS-*b*-PMMA films t_f were determined by subtracting the thickness of the PS-graft layer from the total thickness of the organic film composed of PS-grafted layer and PS-*b*-PMMA layer on the Si substrates. The total thickness of the organic film was measured by removing a portion of the film from the substrate with a sharp knife and measuring the step between the substrate surface and the film surface with a Veeco Nano Scope III atomic force microscope.

2.4. Scanning electron microscope observation

Microdomain structures of PS-*b*-PMMA were observed by using a Hitachi S-4800 field-emission Scanning Electron Microscope (SEM) instrument operated at an acceleration voltage of 0.7 kV. For

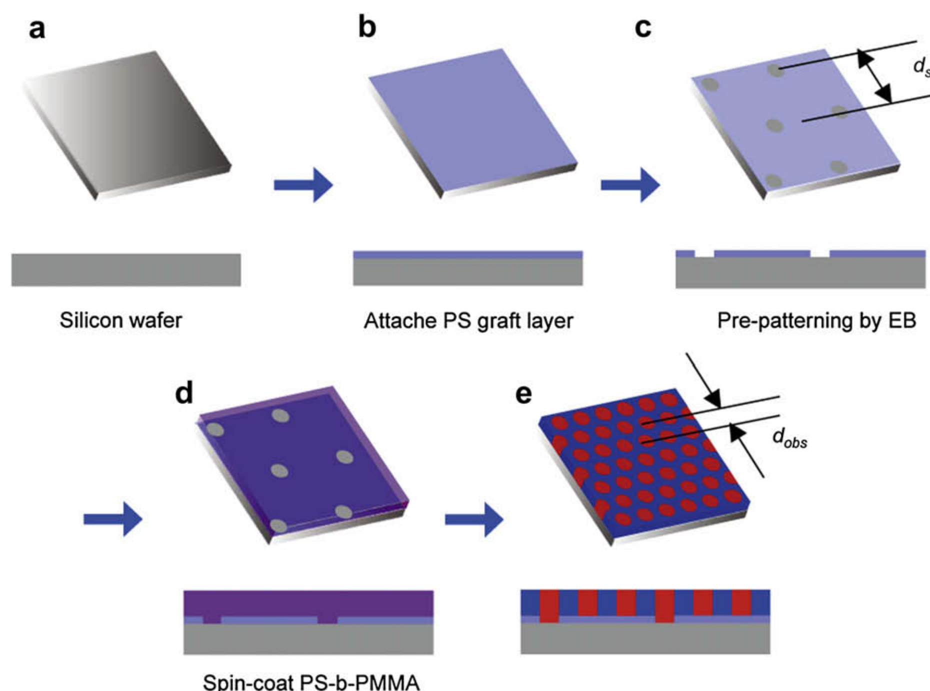

Fig. 1. Schematically illustrated density multiplication process with chemically pre-patterned template.

contrast between the PMMA and PS phases, the block copolymer specimens were etched by O_2 RIE with a SAMCO RIE-10NR. Since the O_2 RIE preferentially etches the PMMA structures, the dark and bright parts of SEM images correspond to PMMA and PS microdomains, respectively.

3. Results and discussion

3.1. Nine-fold density multiplication

Fig. 2(a)–(d) shows the results obtained for nine-fold density multiplication, $d_s = 3d_o$. Fig. 2(a) shows an SEM micrograph of the EB resist pattern employed to prepare the chemical template with $d_s = 72$ nm. Fig. 2(b) shows a SEM image of PS-*b*-PMMA thin film self-assembled on the pre-patterned chemical template. The film thickness of the PS-*b*-PMMA was optimized to $t_f = 38$ nm, which nearly corresponds to $(3/2)d_o$ of the PS-*b*-PMMA block copolymer. The self-assembled film is well-aligned to the template pattern with long-range order in the lattice. Fig. 2(c) is a 2-dimensional fast Fourier transform (2D-FFT) image of Fig. 2(b). Several higher order peaks were observed, with up to 6th order, at $(q/q_m)^2 = 1, 3, 4, 7, 9,$ and 12, with q_m being the 1st order peak position of the 2D-FFT image. From 1st to 3rd order peak positions in the circular averaged 2D-FFT image, the lattice spacing of the self-assembled PMMA cylindrical microdomain was determined to be $d_{obs} = 24$ nm, which was a third of the value of the lattice spacing, $d_s = 72$ nm, of chemically pre-patterned substrate. Fig. 2(d) shows a computer generated image in which the SEM image of the EB resist pattern in orange was superimposed with the SEM image of the directed PS-*b*-PMMA self-assembled pattern in green. This image demonstrates that two PMMA cylinders interpolated linearly between lattice points of the pre-patterned template thus multiplying the feature area density by a factor of 9. To clarify the regularity of the microdomain spacing quantitatively, we calculated standard deviation σ of d spacing for the microdomain of nine-fold density multiplication and compared the results for nine-fold density multiplication with those for four-fold density multiplication and 1:1 correspondence ($d_s = d_o$) from auto-correlation function [27]. It should be noted that the value of σ estimated from auto-correlation function tends to become larger than that estimated from real space analyses though it can express the tendency of the regularity well. The results are shown in Table 1. We also displayed the d spacing and standard deviation of chemical patterns for each condition in Table 1. As for the results for the microdomain, standard deviation for the nine-fold becomes better than the others, although the degree of interpolation is large. This improvement may originate from the fact that the self-assembling of block copolymer becomes dominant in the case of the nine-fold while the chemical pattern having worse standard deviation affects the regularity of the microdomain.

Lithographic applications for high fidelity pattern transfer require a perpendicular orientation of the block copolymer domains. Equilibrium structures of block copolymer thin films including phase

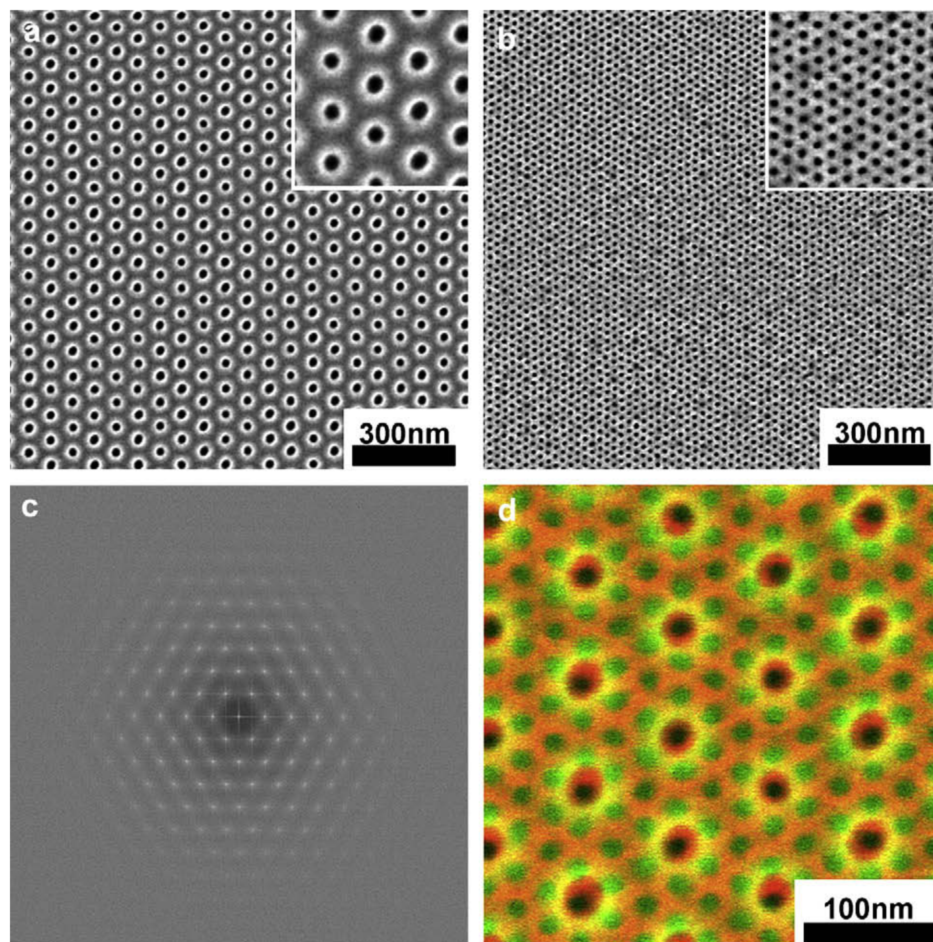

Fig. 2. (a): Top-view SEM image of EB resist employed to pattern PS graft layer on Si wafer surface for a chemically pre-patterned template with $d_s = 72$ nm. (b): Top-view SEM image of cylinder structures of PS-*b*-PMMA with $d_o = 24$ nm self-assembled on the chemically pre-patterned template. Thickness of PS-*b*-PMMA film $t_f = 38$ nm. (c): 2D-FFT image of (b) in arbitrary scale. (d): Computer generated image prepared by over laying (a) and (b) in orange and green, respectively. (For interpretation of the references to color in this figure legend, the reader is referred to the web version of this article.)

Table 1
d and σ for chemical pre-patterns and microdomain of PS-*b*-PMMA.

Configuration	Chemical pre-pattern		PS-*b*-PMMA self-assembly	
	d (nm)	σ (nm)	d (nm)	σ (nm)
1:1 Correspondence ($d_s = d_0$)	23.8	5.3	24.1	2.6
4× Multiplication ($d_s = 2d_0$)	48.4	2.0	23.8	2.6
9× Multiplication ($d_s = 3d_0$)	71.9	2.7	23.8	2.0

morphology and domain orientation are determined by the various parameters that characterize the free energy of a thin film confined between a pre-patterned surface and a top homogenous surface, including annealing temperature, chain conformation, domain–domain interaction, interfacial energies between the block copolymer and the pre-patterned substrate and the free surface (which in turn is determined by the vacuum level and gas composition) [29–33]. The final equilibrium phase morphology and domain orientation correspond to those that minimize the free energy expression [29,33]:

$$F = F_{\text{elastic}} + F_{\text{S-MMA}} + F_{\text{surface}} + F_{\text{interface}} \tag{1}$$

where F_{elastic} being the free energy for the chain conformation, $F_{\text{S-MMA}}$ being the free energy for domain–domain interaction, F_{surface} being the free energy for the free surface, and $F_{\text{interface}}$ being the free energy for the interface between chemically-patterned substrate and PS-*b*-PMMA. The range of thickness values and commensurability tolerance to the chemical pre-pattern for which a perpendicular orientation is more favorable depends on the minimization of the expression in Eq. (1). Keeping interface interactions and the annealing temperature constant, simulations [26,30–32] and experiments [27,30,33] have shown that film thickness and commensurability to d_o span a parameter space where perpendicular orientation is energetically more favorable.

3.2. Effects of thickness of sample on density manipulation

The effect of t_f on nine-fold density multiplication was studied and the results are shown in Fig. 3. The substrate surfaces were patterned with the same template as above with $d_s \approx 3d_o = 72$ nm. Fig. 3(a) and (b) show SEM images of PS-*b*-PMMA thin film self-assembled on the pre-patterned templates with $t_f = 23\ \text{nm} \approx d_o$ and $t_f = 46\ \text{nm} \approx 2d_o$, respectively. In Fig. 3, it is clear that the film thicknesses corresponding to $t_f \approx d_o$ and $t_f \approx 2d_o$, do not show the long-range order exhibited in Fig. 2(b), $t_f \approx (3/2)d_o$. In Fig. 3(a), where $t_f \approx d_o$, the SEM image shows PMMA cylinders both parallel and perpendicular to the substrate surface. In Fig. 3(b), where $t_f \approx 2d_o$, the PMMA cylinders with perpendicular orientation to the substrate surface, but with a poly-grain structure, were observed. The results suggest that when $t_f = 2d_o$, the chemical template pre-pattern does not direct the assembly to the top surface.

The effect of t_f on the cylinder orientation can be discussed in terms of three controlling factors: the conformational entropy of block copolymers (corresponding to F_{elastic}), the interaction between free surface and block copolymers (free surface interaction corresponding to F_{surface}), and the interaction between substrate and block copolymers (substrate interaction corresponding to $F_{\text{interface}}$). The conformational entropy tends to align PMMA cylinders perpendicular [34]. Free surface interaction is almost neutral for both PS and PMMA but varies slightly with annealing temperature and vacuum condition applicable for the experiments. Thus, in principle, free surface interaction induces the cylinder to orient perpendicular to the surface but the strength of free surface interaction depends on the annealing condition. The substrate interaction of the chemically-patterned substrate causes the perpendicular orientation on the lattice points where PS graft layer is etched. However, as for chemical pattern with $d_s = 3d_o$, wide un-etched region with PS graft layer exist in between the etched lattice points. This region favors PS and induces parallel orientation of the PMMA cylinders. In the case of thin samples with $t_f \le d_o$, the substrate interaction becomes dominant rather than the conformational entropy and the free surface interaction. Therefore, many PMMA cylinders are oriented parallel to the surface. On the other hand, as t_f increases, the surface area to volume ratio decreases and the effect of substrate interaction becomes weaker than that for $t_f \le d_o$. Conversely, the effects of the conformational entropy affect the orientation of PMMA cylinders more strongly. Thus, the perpendicular orientation becomes dominant as t_f increases. However, as the effect to register PMMA cylinders on the pre-patterned lattice points are caused by the substrate interaction, the effect diminishes with increasing t_f. Therefore, orientation of hexagonal lattices cannot be directed for thicker samples.

Consideration above suggest that there exist an optimum t_f range for the PMMA cylinders to align perpendicular to the surface and to be directed to form a hexagonal lattice by the substrate pattern. The optimum thickness for complete 9× interpolation was found to be around $t_f = 1.5d_o$ in the experimental conditions we have employed, and agrees with that for 4× interpolation as shown in our previous report [27]. However, the value may change with annealing condition (temperature, degree of vacuum) and/or molecular weights of block copolymers and polymer applied as a graft layer.

3.3. Effects of lattice mismatch on 9× density multiplication

We also investigated the effect of lattice mismatch on the quality of the 9× density multiplication by using chemical pre-patterns slightly below and above the commensurability condition ($d_s = 3d_o = 72$ nm). Fig. 4 shows SEM micrographs and corresponding 2D-FFT images of the microdomain structure of the PS-*b*-PMMA on chemical templates that are slightly mismatched from $3d_o$, namely $d_s = 70\ \text{nm} = 2.9d_o$ and $d_s = 74\ \text{nm} = 3.1d_o$. The PS-*b*-PMMA copolymer film thickness was the prior determined optimal thickness, $t_f = 38$ nm. As can be seen in Fig. 4, regularity and long-range order of PS-*b*-PMMA is worse for the mismatched configurations, than the exact template match, in Fig. 2.

In the case of $d_s = 70$ nm, there are some grains and defects between grains observed in the SEM image (Fig. 4(a-i)). 2D-FFT image displayed a halo pattern suggesting a lack of registration with the surface template (Fig. 4(a-ii)). On the other hand, although grains and defects between grains can be also observed in the SEM image for $d_s = 74$ nm (Fig. 4(b-i)), regularity of the pattern of $d_s = 74$ nm is better than that of $d_s = 70$ nm. The 2D-FFT image (Fig. 4(b-ii)) still shows a hexagonal pattern reflecting the single orientation of the domain structure, though the peaks are broader than that of $d_s = 72$ nm (Fig. 2). The lattice spacing of the domain structure determined from the 2D-FFT image for $d_s = 74$ nm was $d_{\text{obs}} = 25$ nm, indicating that the diblock copolymer chains are slightly extended to follow the chemical pattern of the template. The difference in the FFT patterns between $d_s = 70$ nm and $d_s = 74$ nm indicates that compression of the PS-*b*-PMMA chains is energetically unfavored in comparison to the case of stretching. This tendency have been shown for the chemical registration of PS-*b*-PMMA lamella [23] and cylindrical morphologies for $d_s \approx d_o$ [27,33], and for the 4× density multiplication of PS-*b*-PMMA cylindrical morphology with $d_s \approx 2d_o$ [27]. However, the tolerance of the mismatch for nine-fold density multiplication is smaller than that for four-fold density multiplication.

The effect of commensurability is interpreted as a thermodynamic competition between the interfacial free energy gain in aligning the diblock copolymer microdomains with the surface

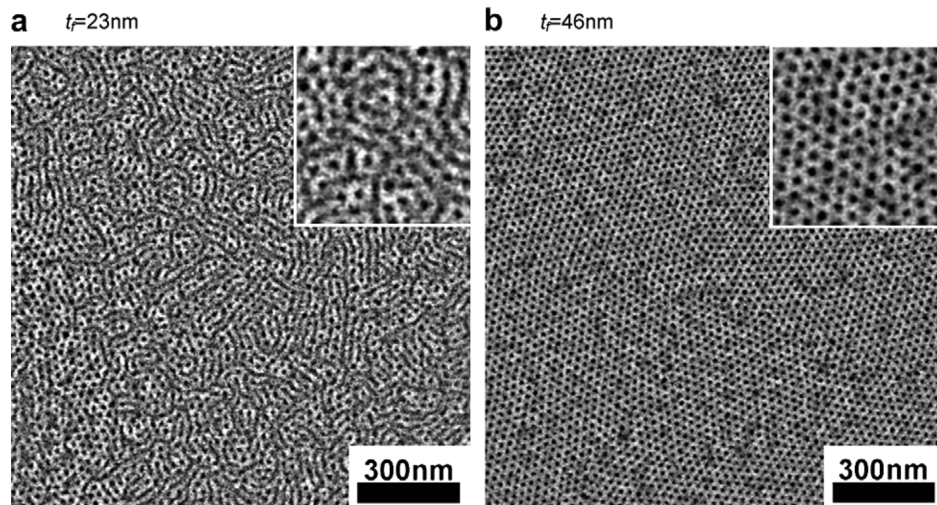

Fig. 3. Top-view SEM images of cylinder structures of PS-*b*-PMMA with $d_o = 24$ nm self-assembled on the chemically pre-patterned template with $d_s = 72$ nm. Thickness of PS-*b*-PMMA film: (a) $t_f = 23$ nm and (b) $t_f = 46$ nm.

template, and the loss of conformational entropy as the chains stretch or compress to achieve the template lattice spacing. In most cases, surface interaction enthalpy dominates to maintain single crystal-like structure up to about 6–10% stretch of the lattice spacing d_o in the case of $d_s \approx d_o$ [23,27,33]. In comparison, the result presented in Fig. 4(b-i) and (b-ii) demonstrates that PS-*b*-PMMA cannot maintain a defect-free lattice on $d_s = 74$ nm. The increase in the lattice spacing from its natural value of $d_o = 24$ nm to self-assembled value of $d_{obs} = 25$ nm on the substrate of $d_s = 74$ nm corresponds to about 4% stretch in d_o, which is considerably smaller than the critical value for the mismatch in the case of 4× density multiplication with $d_s \approx 2d_o$ [27]. The number of pre-patterned lattice points for $d_s \approx 3d_o$ is 1/9 of that for $d_s \approx d_o$ and 4/9 of that for $d_s \approx 2d_o$. Although further systematic work is required, observed

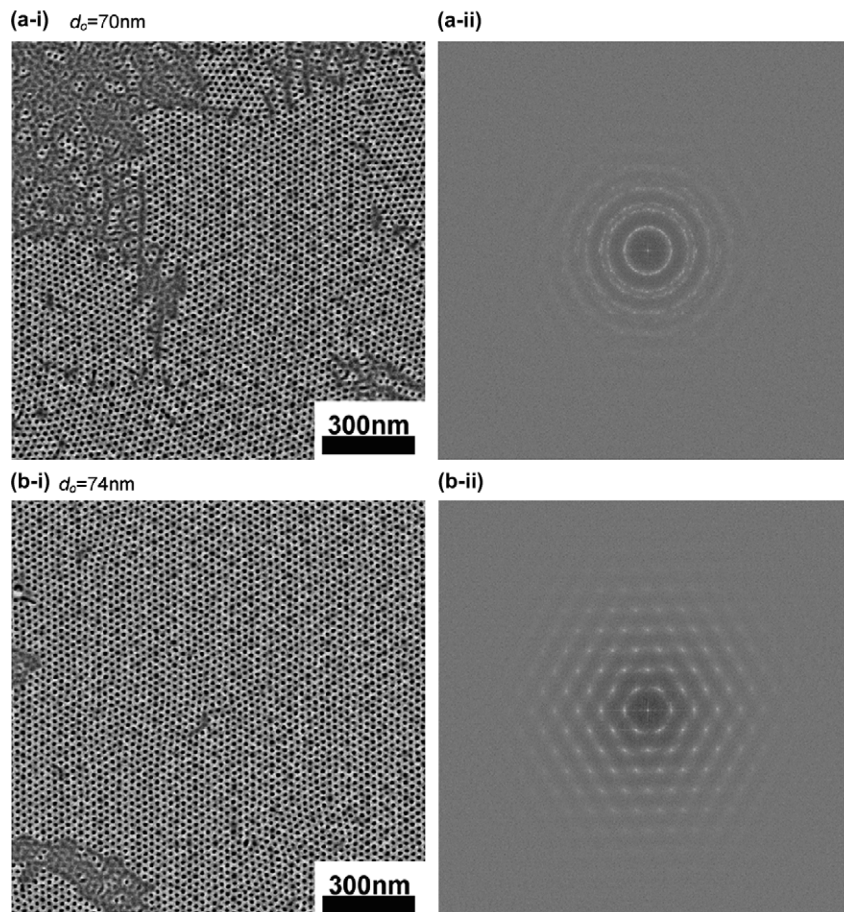

Fig. 4. Top-view SEM images of cylinder structures of PS-*b*-PMMA with $d_o = 24$ nm self-assembled on the chemically pre-patterned template with (a-i) $d_s = 70$ nm and (b-i) $d_s = 74$ nm. (a-ii) and (b-ii) display 2D-FFT images of (a-i) and (b-i), respectively in arbitrary scale. Thickness of PS-*b*-PMMA film: $t_f = 38$ nm.

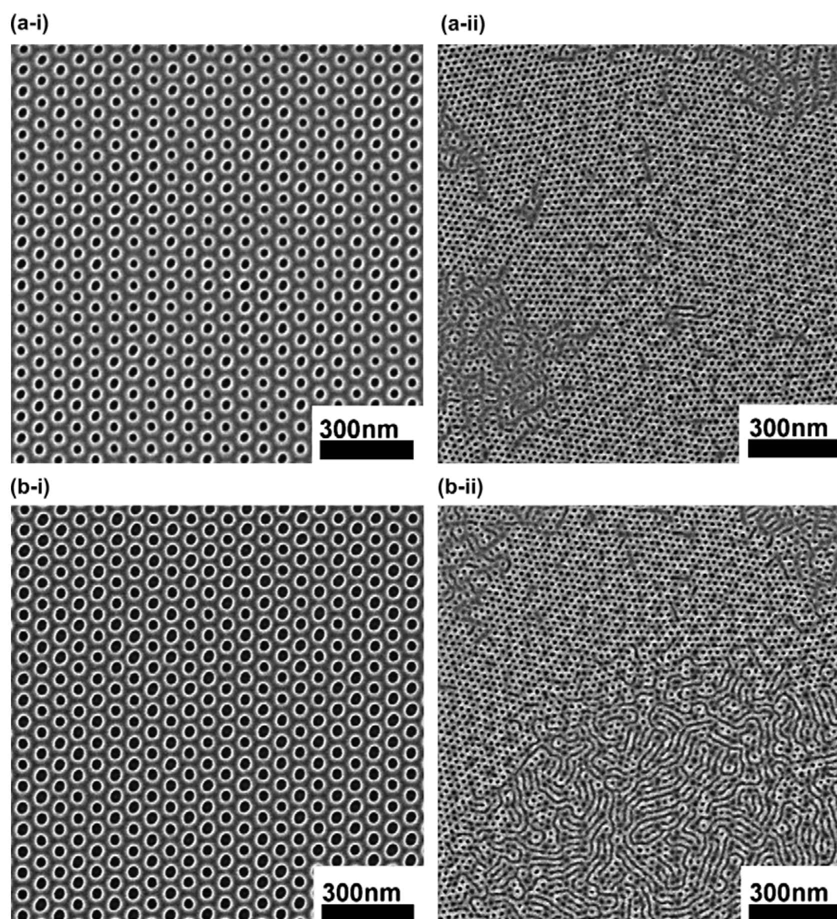

Fig. 5. (a-i) and (b-i): Top-view SEM images of EB resist employed to pattern PS graft layer on Si wafer surface for a chemically pre-patterned template with $d_s = 72$ nm. (a-ii) and (b-ii): Top-view SEM images of cylinder structures of PS-*b*-PMMA with $d_o = 24$ nm self-assembled on the chemically pre-patterned template prepared by applying EB mask shown in (a-i) and (b-i), respectively. Thickness of PS-*b*-PMMA film: $t_f = 38$ nm.

results can be attributed to relatively smaller gain in surface interaction enthalpy to overcome the conformational entropy loss of block copolymer chains for $d_s \approx 3d_o$ compared to that for $d_s \approx d_o$ and $d_s \approx 2d_o$.

3.4. Effects of size of chemical pattern points on 9× density multiplication

Lastly, the effect of size of chemical template lattice points on the self-assembly is examined. As can be clearly seen in Fig. 2(d), radius of the holes of resist pattern prepared by EB lithography r_{EB} was larger than that of the PMMA cylindrical microdomain self-assembled on the template r_{obs}. The r_{EB} and r_{obs} measured from SEM micrographs presented in Fig. 2(a) and (b) were 11 nm and 6 nm, respectively. To investigate the limitation of r_{obs}/r_{EB}, chemical templates were prepared by using resist patterns with larger r_{EB} and PS-*b*-PMMA was conducted to self-assembled on them. Results are presented in Fig. 5. Fig. 5(a-i) and (b-i) displays SEM images of resist pattern with $r_{EB} = 13$ nm and 19 nm, respectively. Fig. 5(a-ii) and (b-ii) displays SEM images of PS-*b*-PMMA self-assembled film with $t_f = 38$ nm on the chemically pre-patterned templates prepared from the resist patterns in Fig. 5(a-i) and (b-i), respectively. As can be seen, with increasing r_{EB}, regions with cylinders parallel to the substrate are shown in the SEM images of the self-assembled block copolymer. The areal regions of cylinders parallel to the substrate increased with increasing template point size. In addition, 2D-FFT image obtained from the region with perpendicularly oriented cylinders displayed a halo pattern (not shown) suggesting that the pre-pattern underneath had limited influence on the arrangement of PMMA cylindrical microdomains. In spite of the changes in PMMA cylindrical microdomain formation, the radii of perpendicularly oriented PMMA cylindrical microdomains remained almost constant at $r_{obs} = 6$ nm and independent of r_{EB}. The increase in r_{EB} tends to enlarge r_{obs} to minimize the substrate interaction. However, the increase of r_{obs} is unfavorable in terms of the conformational entropy of PMMA chains. Thus, to compensate the substrate interaction and the conformational entropy, the cylinders tend to align parallel to the substrate.

4. Conclusion

We have demonstrated a nine-fold feature density multiplication by EB directed block copolymer assembly that enhances both resolution and throughput of the EB-generated patterns providing a feasible path to fabricating master molds of nanometer scale patterns over macroscopic areas. We have found that the equilibrium formation of perpendicular cylindrical domains in registration with the pre-patterned surface is confined within a narrow thickness and commensurability range as observed in previous simulations and experiments with lower density multiplication factors. As for lattice mismatch between chemical pattern and *d* spacing of domains, compression of the PS-*b*-PMMA chains is energetically unfavored in comparison to the case of stretching. This tendency has been shown for the four-fold feature density multiplication. However, the tolerance of the mismatch for nine-fold feature

density multiplication is smaller than that for four-fold feature density multiplication. We also show that the critical dimension formed by the block copolymer domains is independent of that defined by the EB pre-patterned features bringing a reliable method for CD control at sub-lithographic resolutions. Viewed from the opposite side, these results indicate that the chemical registration of PS-*b*-PMMA cannot only reduce the lattice spacing but also reduce the pattern radius. Current photolithographic technology utilizes projection exposure to transfer mask pattern in reduced size to the resist. The present results indicate that directed self-assembly can provide alternative route to reduce pattern to the size which cannot be achieved by the current lithography due to the diffraction limit. It should be noted that Stoykovich et al. have successfully directed block copolymers to self-assembled into various isolated patterns applicable for integrated circuit by registering the lamella microdomains one-to-one on the chemical pre-pattern by applying block copolymer/homopolymer blend systems [35]. Although present experiments were performed for hcp regular pattern, their results strongly support the possibility to adapt the presented technique to more complex configurations.

References

[1] Smith BW, Bourov A, Kang H, Cropanese F, Fan Y, Lafferty N, Zavyalova, L. Proc SPIE 2004;273:5377.
[2] Terris BD, Thomson T. J Phys D Appl Phys 2005;38:R199.
[3] Muray A, Scheinfein M, Isaacson M, Adesida IJ. Vac Sci Technol 1985;B3:367.
[4] Yasin S, Hasko DG, Ahmed H. Microelectron Eng 2002;61–62:745.
[5] Yang XM, Xiao S, Wu W, Xu Y, Lee K, Kuo D, et al. Vac Sci Technol 2007;B25:2202.
[6] Park C, Yoon J, Thomas EL. Polymer 2003;44:6725.
[7] Hamley IW. Angew Chem Int Ed 2003;42:1692.
[8] Segalman RA. Mater Sci Eng R 2005;48:191.
[9] Hawker CJ, Russell TP. MRS Bull 2005;30:952.
[10] Stoykovich MP, Nealey PF. Mater Today 2006;9:20.
[11] Khandpur AK, Forster S, Bates FS, Hamley IW, Ryan AJ, Bras W, et al. Macromolecules 1995;28:8796.
[12] Bates FS, Fredrickson GH. Annu Rev Phys Chem 1990;41:525.
[13] Hashimoto T. In: Legge NR, Holden G, Schroeder HE, editors. Thermoplastic elastomers. Vienna: Hanser; 1996.
[14] Matsen MW, Schick M. Phys Rev Lett 1994;72:2660.
[15] Takenaka M, Wakada T, Akasaka S, Nishitsuji S, Saijo K, Shimizu H, et al. Macromolecules 2007;40:4399.
[16] Black CT, Guarini KW, Milkove KR, Baker SM, Russell TP, Tuominen MT. Appl Phys Lett 2001;79:409.
[17] Segalman RA, Yokoyama H, Kramer EJ. Adv Mater 2001;13:1152.
[18] Sundrani D, Sibener SJ. Macromolecules 2002;35:8531.
[19] Cheng JY, Mayes AM. Nat Mater 2004;3:823.
[20] Xiao SG, Yang XM, Edwards EW, La YH, Nealey PF. Nanotechnology 2005;16: S324.
[21] Chen F, Akasaka S, Inoue T, Takenaka M, Hasegawa H, Yoshida H. Macromol Rapid Commun 2007;28:2137.
[22] Rockford L, Liu Y, Mansky P, Russell TP, Yoon M, Mochrie SG. J Phys Rev Lett 1999;82:2602.
[23] Kim SO, Solak HH, Stoykovich MP, Ferrier NJ, de Pablo JJ, Nealey PF. Nature 2003;424:411.
[24] Edwards EW, Stoykovich MP, Solak HH, Nealey PF. Macromolecules 2006;39: 3598.
[25] Welander AM, Kang H, Stuen KO, Solak HH, Müller M, de Pablo JJ, et al. Macromolecules 2008;41:2759.
[26] Ruiz R, Kang H, Detcheverry FA, Dobisz E, Kercher DS, Alberecht TR, et al. Science 2008;321:936.
[27] Tada Y, Akasaka S, Yoshida H, Hasegawa H, Dobisz E, Kercher D, et al. Macromolecules 2008;41:9267.
[28] Cheng JY, Rettner CT, Snaders DP, Kim HC, Hinsberg WD. Adv Mater 2008;20:3155.
[29] Edwards EW, Montague MF, Solak HH, Hawker CJ, Nealey PF. Adv Mater 2004;16:1315.
[30] Wang Q, Nath SK, Graham MD, Nealey PF, de Pablo JJ. J Chem Phys 2000;112:9996.
[31] Wang Q, Nealey PF, de Pablo JJ. Macromolecules 2001;34:3458.
[32] Wang Q, Nealey PF, de Pablo JJ. Macromolecules 2003;36:1731.
[33] Park SM, Craig GSW, Liu CC, La YH, Ferrier NJ, Nealey PF. Macromolecules 2008;41:9118.
[34] Pickett GT, Witten TA, Nagel SR. Macromolecules 1993;26:3194.
[35] Stoykovich MP, Kang H, Daoulas KC, Lui G, Liu C-C, de Pablo JJ, et al. ACS Nano 2007;1:168.